Available online at www.sciencedirect.com
ScienceDirect
Trans. Nonferrous Met. Soc. China 22(2012) 268−274
Transactions of Nonferrous Metals Society of China
www.tnmsc.cn

Quench sensitivity and microstructure character of high strength AA7050

LI Pei-yue[1,2], XIONG Bai-qing[2], ZHANG Yong-an[2], LI Zhi-hui[2], ZHU Bao-hong[2], WANG Feng[2], LIU Hong-wei[2]

1. Luoyang Ship Material Research Institute, Luoyang 471003, China;
2. State Key Laboratory of Nonferrous Metals and Processes, General Research Institute for Nonferrous Metals, Beijing 100088, China

Received 17 January 2011; accepted 26 October 2011

Abstract: The effect of quenching rate on the electrical conductivity and microstructure of thick plates of incumbent AA7050 was investigated by employing Jominy end quench test. The electrical conductivity measurement and microstructural observation were conducted at different distances from the quenched end. The results indicate that the average cooling rates decrease with increasing the distance from the quenched end of the bar in the quench sensitive temperature range. However, the electrical conductivity increases with the increase of distance from the quenched end. The surface parts of the plate were fully recrystallized, while partial recrystallization took place at the quarter and center parts of the plate. The quench induced grain boundary precipitates became remarkably coarser and discontinuously distributed with increasing distance from the quenched end of the bar. Plenty of heterogeneous precipitates were observed to nucleate on Al_3Zr dispersoids when the distance from the quenched end was greater than 38 mm.

Key words: Jominy end quench test; quench sensitivity; cooling rate; quench induced precipitates

1 Introduction

The Al−Zn−Mg−Cu (7xxx series) alloys are extensively used in the commercial aircraft structures as well as various critical military bridges and vehicles due to their excellent mechanical properties developed during the age-hardening process, high specific strength, fracture toughness and SCC resistance [1, 2]. One of the problems arising in the heating treatment of the ultra thick plates during the solution and quenching treatment is the quench sensitivity, which brings on the inhomogeneity and reduction in properties in the center of the plates [3−5]. For its practical importance, many investigations have been done on the quench sensitivity of Al−Zn−Mg−Cu alloys for the urgent demands of integral structures [6−8].

In aluminum alloys, there is desire to determine the effect of quenching on the microstructure and final properties after a certain aging treatment. The Jominy end quench test, well known as a method of measuring hardenability in steels, offers a method for studying many quenching conditions with a minimum amount of samples [9, 10]. The aim of the present work concerns the relationship between the cooling rate and the microstructure, electrical conductivity of a 152.4 mm thick commercial 7050 aluminum alloy plate by using the Jominy end quench test. The potential for developing a new understanding of the complex response of nonferrous alloys under processing conditions, especially quenching, were presented [9].

2 Experimental

The composition of the main alloying elements of AA7050 is listed in Table 1. The 7050 ingots with 440 mm in thickness were made by DC casting, milled to 400 mm and then hot rolled to 152.4 mm at 420−430 °C after homogenization treatment.

A bar with size of *d*48 mm×152.4 mm was taken along the short direction of the plate. Small holes were drilled at 5, 10, 35, 60, 85 and 135 mm respectively from the quenched end in order to introduce a group of 1.5 mm-diameter K thermocouples inserted with their tips at the mid-point of the bar. A computer-driven MX100 data logging system was employed to record the

Foundation item: Project (50904010) supported by the National Natural Science Foundation of China; Project (2010DFB50340) supported by the China International Science and Technology Cooperation
Corresponding author: LI Pei-yue; Tel: +86-379-67256964; E-mail: lpy110015@163.com
DOI: 10.1016/S1003-6326(11)61170-9

Table 1 Main elemental composition of studied alloy (mass fraction, %)

Zn	Mg	Cu	Zr
6.43	2.3	2.19	0.11
Fe	Si	Mn	Al
0.11	0.025	<0.01	Bal.

heating and cooling curves. The bar was soaked in a Muffle furnace at 470 °C for 50 min, ramped to 485 °C in 60 min, and then held for 90 min to allow more elements to go back to the matrix. After the solution treatment, the bar was transferred to a set of Jominy end quench test equipment within 5 s. Water was sprayed to the quenched end from a pipe immediately. The free height of the water was kept 120 mm during the whole quenching process. The switch of water was turned off until the temperature of the bar was below 50 °C.

The electrical conductivity of the as-quenched bar was measured using WD-Z digital eddy current conductivity meter (measuring in the unit of $MS \cdot m^{-1}$), which was calibrated with a test block. The microstructures of alloys at distance of 0, 38, 76 and 100 mm from the quenched end of the bar were investigated using Zeiss Axiovert 200MAT optical microscope. Specimens were polished and etched in Graff Sergeant's reagent (84 mL water, 15.5 mL HNO_3, 0.5 mL HF and 3 g CrO_3) to show the grain structure. Specimens for TEM observation were thinned by electropolishing using a twin-jet polisher with a 25% nitric acid in methanol at −30 °C and 15−20 V. The specimens were examined by bright field imaging in a JEOL 2010FX microscope operated at 200 kV.

3 Results and discussion

3.1 Cooling curves

The quenched end of the bar was polished before the experiment to reduce the effect of the oxide on the heat transfer process. Figure 1 shows the thermal evolution of the bar during quenching process and the average cooling rates as a function of distance from the quenched end of the bar in the quench sensitive temperature range (450−250 °C [11]). The distances corresponding to the positions are measured from the quenched end, at which the thermocouples are located. It can be found that the cooling rates decrease during the quench process. The temperature of the quenched end is at a lower range in a short time, while it takes longer time for the alloys away from the quenched end below 200 °C (Fig. 1(a)). In Fig. 1(b), the cooling rates of the bar decrease with increasing distance from the quenched end. The average cooling rates of the alloys at 5, 10, 35, 60, 85 and 135 mm from the quenched end in the quench sensitive temperature range (450−250 °C) are 25.94, 17.26, 4.69, 2.30, 1.72 and 1.53 K/s, respectively. The cooling rate exhibits an evident decrease during the first 60 mm from the quenched end before a plateau is reached. The Jominy end quench test is designed to simulate the one dimension cooling of thick and ultra-thick plates in factories. The surface part of the quenched bar is cooled to a lower temperature after the spring of the cooling water, but the alloys away from the quenched end are at solution temperature, so a large temperature gradient is formed, which decreases with the distance from the quenched end. The larger the temperature gradient is, the more the heat flows and the higher the cooling rate is. So the cooling rates of the bar decrease with the increase of the distance from the quenched end and have a similar value when the temperature gradient is small.

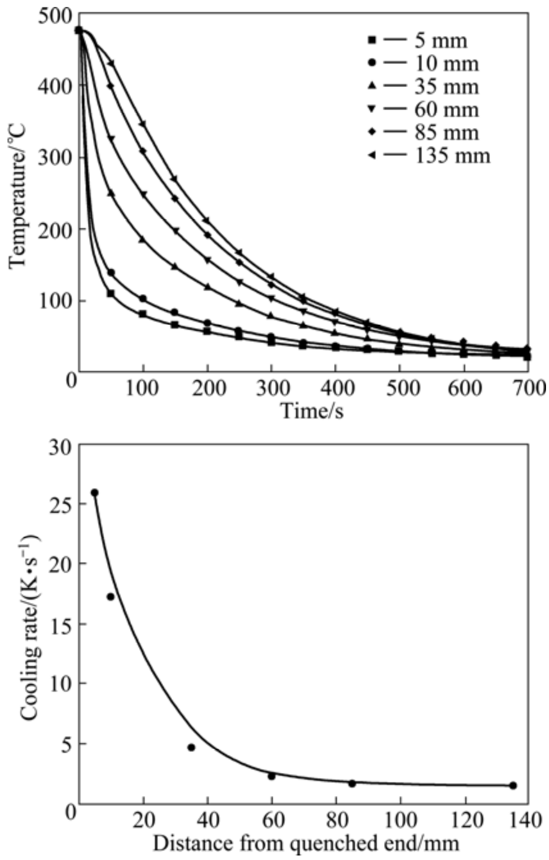

Fig. 1 Cooling curves (a) and average cooling rates as function of distance from quenched end of bar (b) in quench sensitive temperature range (450−250 °C)

3.2 Electrical conductivity curve

Pieces were sliced at different distances from the quenched end and the electrical conductivity of the as-quenched bar was measured. The results are shown in Fig. 2. It can be observed that the electrical conductivity increases with increasing the distance from the quenched

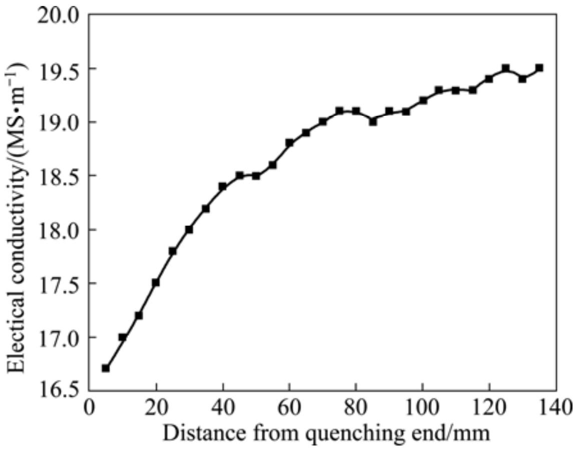

Fig. 2 Electrical conductivity as function of distance form quenched end of as-quenched bar

end, which soars up in the first 75 mm. It is consistent with the appearance of the variation of average cooling rates in Fig.1 (b) to some extent. The electrical conductivity can be used to reflect the supersaturation of the solid solution [12]. The solid solution decomposes when the cooling rate is smaller than a critical value. And the lower the cooling rate is, the higher level it decomposes. Changes in the electrical conductivity of the as-quenched bar can be rationalized by the decreased density of quenched-in vacancies and solute in the matrix of the bar, which is determined by the quenching process.

3.3 Microstructural characterization

3.3.1 Optical microscope

Figure 3 shows the optical microstructures of the

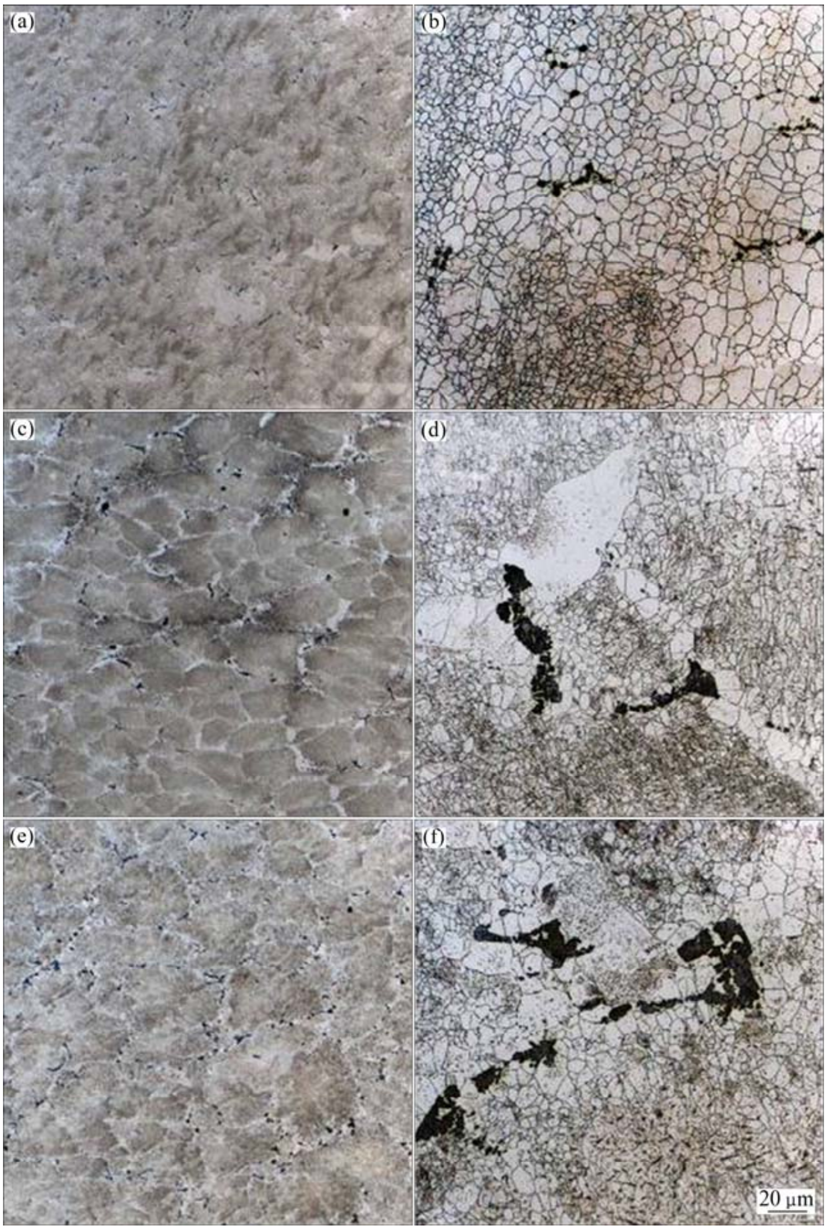

Fig. 3 Optical microstructures of as-aged bar at distance of 0 mm (a, b), 35 mm (c, d) and 75 mm (e, f) from quenched end

as-aged bar. From Figs. 3(a) and (b), it can be found that alloy at 0 mm from the quenched end (the surface parts of the 152.4 mm-thick plate) is fully recrystallized, the grains are 1−25 μm in size, most of which are bigger than 10 μm. Partial recrystallization takes place at the quarter height of the bar (the quarter thickness of the 152.4 mm-thick plate) with recrystallized grain size smaller than 10 μm (Figs. 3 (c) and (d)). The microstructure of the alloy at 75 mm from the quenched end (the center part of the 152.4 mm-thick plate) is similar to the quarter one, with many recrystallized grains smaller than 10 μm in size, albeit some abnormal grown grains with residual particles in them (Figs. 3 (e) and (f)). Heterogeneous microstructures from the surface to the center of the thick plate, which influences the precipitate inevitably during aging, have an effect on the properties of the plate, giving rise to the quench sensitivity of the plate finally.

3.3.2 TEM observation of as-quenched bar

The bright field TEM images and selected area electron diffraction patterns in the $\langle 112\rangle_{Al}$ projection of the as-quenched bar are shown in Fig. 4. The morphology and distribution of precipitates in the as-quenched bar are displayed in Figs. 4(a) and (c). A rather homogeneous distribution of the precipitated particles is found with a mean diameter of 10−15 nm after solution and subsequent water quenching. As shown in the SAED patterns in Figs. 4(b) and (d), spherical Al_3Zr spots can be clearly identified. Diffuse spots near $1/2\{311\}_{Al}$ associated with the GP II zones are clearly observed, and the diffraction features of η' phases are also observed, such as some diffraction spots and stronger streaks along {111} direction at 1/3 and 2/3 of the {220} positions [13, 14]. This indicates that both GP II zones and η' phases are therefore present in the as-quenched bar.

Figure 5 illustrates the morphology and distribution of the grain boundary precipitates (η phases) of the as-quenched bar. With increasing distance from the quenched end of the bar, the grain boundary precipitates become remarkably coarser and discontinuously distributed, and the width of the precipitates increases obviously as the distance increases from 38 to 100 mm.

Figure 6 shows the TEM images of the subgrain

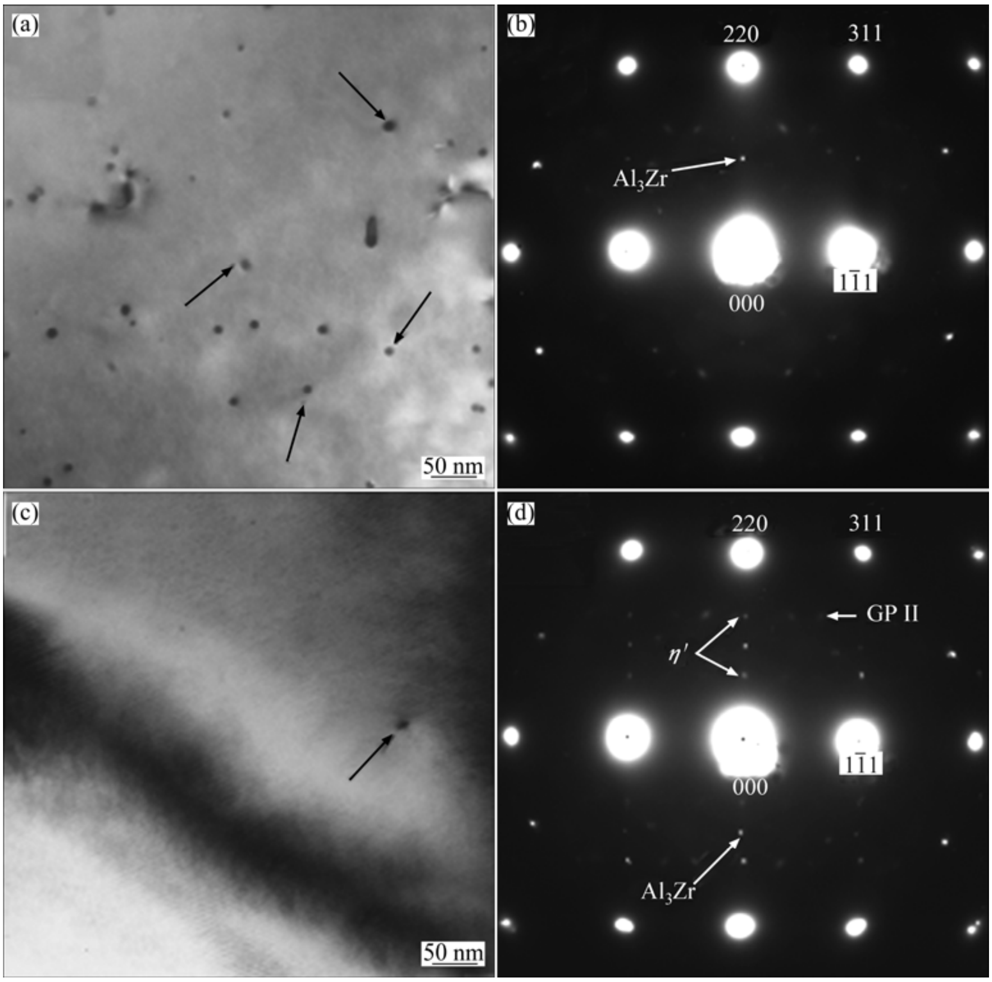

Fig. 4 Bright field TEM images and corresponding SAED patterns in alloys at distance of 0 mm (a, b) and 70 mm (c, d) from quenched end after solution treatment and water quenching

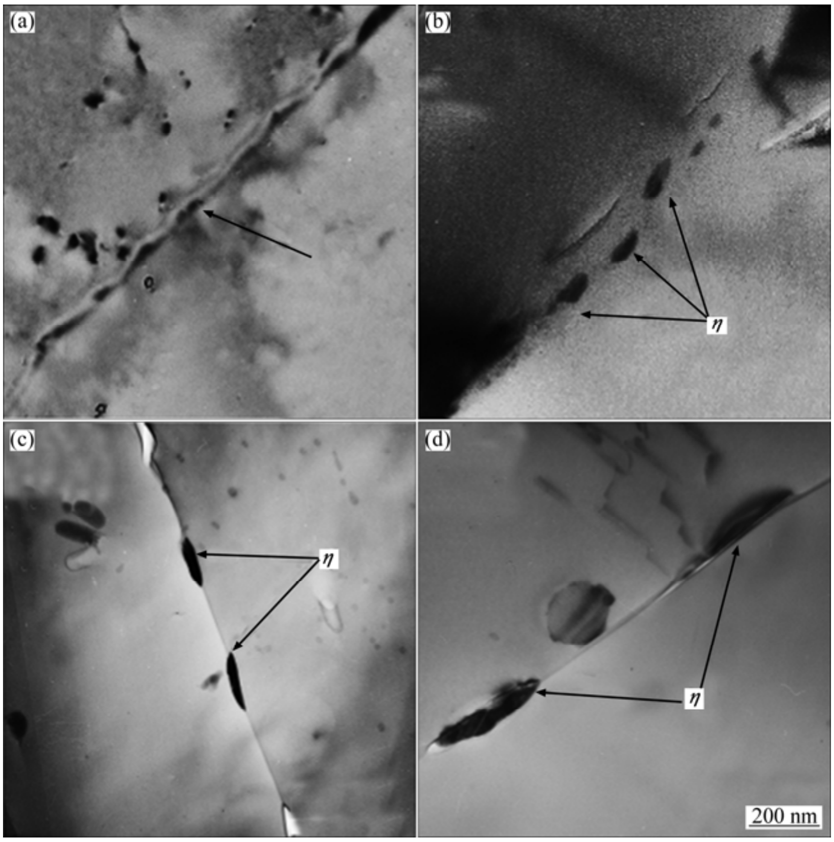

Fig. 5 TEM images of grain boundary precipitates at distance of 0 mm (a), 38 mm (b), 70 mm (c) and 100 mm (d) from quenched end of as-quenched bar

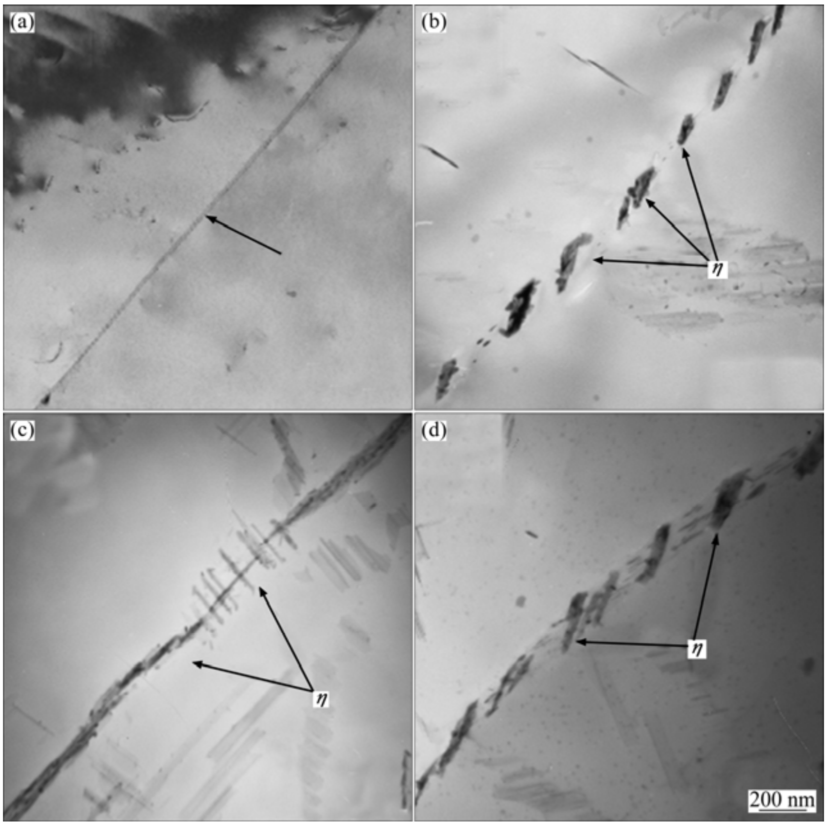

Fig. 6 TEM images of subgrain boundary precipitates at distance of 0 mm (a), 38 mm (b), 70 mm (c) and 100 mm (d) form quenched end of as-quenched bar

boundary precipitates of the as-quenched bar. It can be found that the subgrain boundary at 0 mm from the quenched end in Fig. 6(a) displays few η phases at that the cooling rate above the critical rate of the alloy. While irregular morphology and distribution of the subgrain boundary precipitate (η phases) are clearly observed when the distance is above 38 mm.

Figure 7 represents the TEM images of the quench-induced precipitation in grains of the as-quenched bar. It is observed in Fig. 7 that plenty of heterogeneous precipitates during the quench mostly nucleate on Al_3Zr dispersoids when the distance from the quenched end is above 38 mm. The aspect ratio of the precipitation is small with size of 100−500 nm. The η precipitates grow in the long direction, albeit that the number of the precipitates decreases with the increase of the distance.

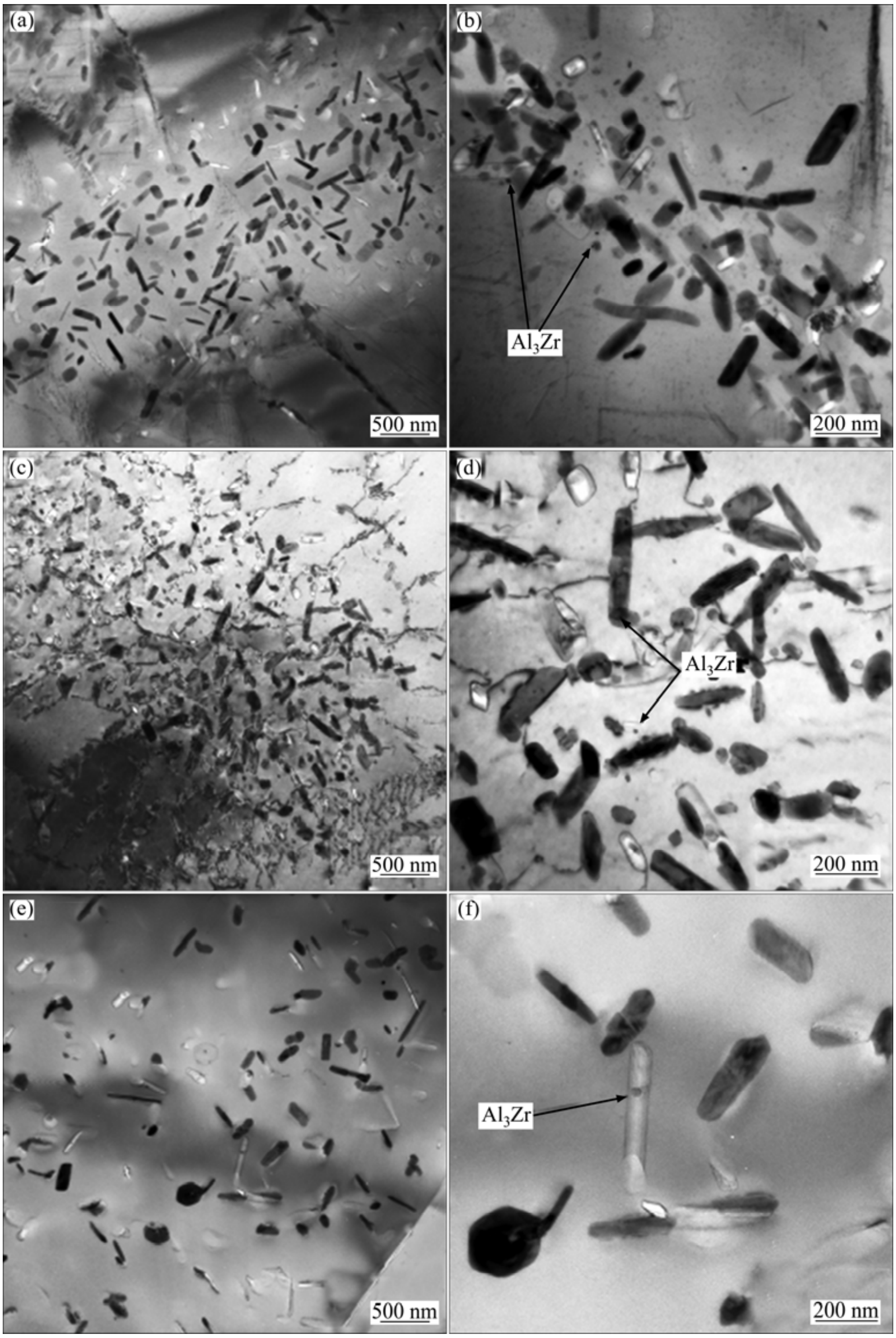

Fig. 7 TEM images of quench-induced precipitation in grains at distance of 38 mm (a, b), 70 mm (c, d) and 100 mm (e, f) from quenched end of as-quenched bar

It takes 8, 42 and 87 s for the alloys at 5, 35 and 60 mm from the quenched end to get through the quench sensitive temperature range, respectively. The supersaturated solid solution decomposes at the defects of the matrix, grain boundary, sub-grain boundary and Al_3Zr dispersoids [15]. The size and volume of the quench induced precipitates grow with the dwell in the quench sensitive temperature range, and the supersaturation of the solid solution decreases. The electrical conductivity increases with the increase of distance from the quenched end.

4 Conclusions

1) The average cooling rates decrease with increasing the distance from the quenched end of the bar in the quench sensitive temperature range (450−250 °C).

2) The grain boundary precipitates become remarkably coarser and discontinuously distributed with increasing the distance from the quenched end of the bar.

3) Plenty of heterogeneous precipitates are observed to nucleate on Al_3Zr dispersoids when the distance from the quenched end is above 38 mm.

References

[1] CHAKRABARTI D J, LIU J, SAWTELL R R, VENEMA G B. New generation high strength high damage tolerance 7085 thick alloy product with low quench sensitivity [J]. Materials Forum, 2004, 28: 969−974.

[2] HILPERT M, TERLINDE G, EITULSKI T, VUGRIN T, KNÜWER M. AA7037—A new high strength aluminum alloy for aerospace applications [C]//HIRSCH J, SKROTZKI B, GOTTSTEIN G. Proceedings of the 11th International Conference on Aluminium Alloys. Weinheim: WILEY-VCH Verlag GmbH & Co. KGaA, 2008: 209−214.

[3] DUMONT D, DESCHAMPS A, BRÉCHET Y, SIGLI C, EHRSTRÖM J C. Characterisation of precipitation microstructures in aluminium alloys 7040 and 7050 and their relationship to mechanical behaviour [J]. Materials Science and Technology, 2004, 20: 567−576.

[4] LIM S T, YUN S J, NAM S W. Improved quench sensitivity in modified aluminum alloy 7175 for thick forging applications [J]. Materials Science and Engineering A, 2004, 371(1−2): 82−90.

[5] DESCHAMPS A, TEXIER G, RINGVAL S, DELFAUT-DURNT L. Influence of cooling rate on the precipitation microstructure in a medium strength Al–Zn–Mg alloy [J]. Materials Science and Engineering A, 2009, 501: 133−139.

[6] CONSERVA M, RUSSO E D, CALONI O. Comparison of the influence of chromium and zirconium on the quench sensitivity of Al−Zn−Mg−Cu alloys [J]. Metallurgical and Materials Transactions B, 1971, 2: 1227−1232.

[7] ROBINSON J S, CUDD R L, TANNER D A, DOLAN G P. Quench sensitivity and tensile property inhomogeneity in 7010 forgings [J]. Journal of Materials Processing Technology, 2001, 119: 261−267.

[8] LIU S D, ZHONG Q M, ZHANG Y, LIU W J, ZZHANG X M, DENG Y L. Investigation of quench sensitivity of high strength Al−Zn−Mg−Cu alloys by time−temperature−properties diagrams [J]. Materials and Design, 2010, 31: 3116−3120.

[9] NEWKIRK J W, MACKENZIE D S. The Jominy end quench for light-weight alloy development [J]. Journal of Materials Engineering and Performance, 2000, 9: 408−415.

[10] MACKENZIE D S, NEWKIRK J W. Heat treatment optimization of 7××× aluminum alloy [C]//TIRYAKIOGLU M. Proceedings of Materials Solutions Conference. 2001, 8: 57−62.

[11] ZHANG Xin-ming, LIU Wen-jun, LIU Sheng-dan, YUAN Yu-bao, DENG Yun-lai. TTP curve of aluminum alloy 7050 [J]. The Chinese Journal of Nonferrous Metals, 2009, 19(5): 861−868. (in Chinese)

[12] XIONG Bo-qing, LI Xi-wu, ZHANG Yong-an, LI Zhi-hui, ZHU Bao-hong, WANG Feng, LIU Hong-wei. Novel Al−7.5Zn−1.65Mg−1.4Cu−0.12Zr alloys with high strength high toughness and low quench sensitivity [J]. The Chinese Journal of Nonferrous Metals, 2009, 19(9): 1539−1547. (in Chinese)

[13] BERG L K, GJØNNES J, HANSEN V, LI X Z, KNUTSON-WEDEL M, WATERLOO G, SCHRYVERS D, WALLENBERG L R. GP-zones in Al–Zn–Mg alloys and their role in artificial aging [J]. Acta Materialia, 2001, 49: 3443−3451.

[14] SHA G, CEREZO A. Early-stage precipitation in Al−Zn−Mg−Cu alloy (7050) [J]. Acta Materialia, 2004, 52(15): 4503−4516.

[15] GODARD D, ARCHAMBAULT P, AEBY-GAUTIER E, LAPASSET G. Precipitation sequences during quenching of the AA 7010 alloy [J]. Acta Materialia, 2002, 50: 2319−2329.

7050 高强铝合金淬火敏感性及组织特征

李培跃 [1,2]，熊柏青 [2]，张永安 [2]，李志辉 [2]，朱宝宏 [2]，王 锋 [2]，刘红伟 [2]

1. 洛阳船舶材料研究所，洛阳 471003;

2. 北京有色金属研究总院 有色金属材料及制备国家重点实验室，北京 100088

摘 要：采用 Jominy 末端淬火实验研究淬火冷却速率对商用 7050 铝合金厚板淬火态合金电导率和组织的影响。实验测定距淬火端不同距离合金的淬火态电导率，并进行组织观察。结果表明：在淬火敏感区间范围内，合金的平均冷却速率随着淬火端距离的增加不断降低，而淬火态合金的电导率随着距离的增加不断上升。末端淬火实验棒组织观察显示，厚板表面已发生完全再结晶，1/4 和 1/2 厚度处为部分再结晶组织，淬火诱导晶界析出相逐渐粗化并成链状分布，当距离大于 38 mm 时，发现大量非均质形核淬火析出相，其形核核心主要为 Al_3Zr 弥散相。

关键词：Jominy 末端淬火；淬火敏感性；冷却速率；淬火诱导析出相

(Edited by FANG Jing-hua)